iScience

CellPress

Article

# Microglia Induce PDGFRB Expression in Glioma Cells to Enhance Their Migratory Capacity

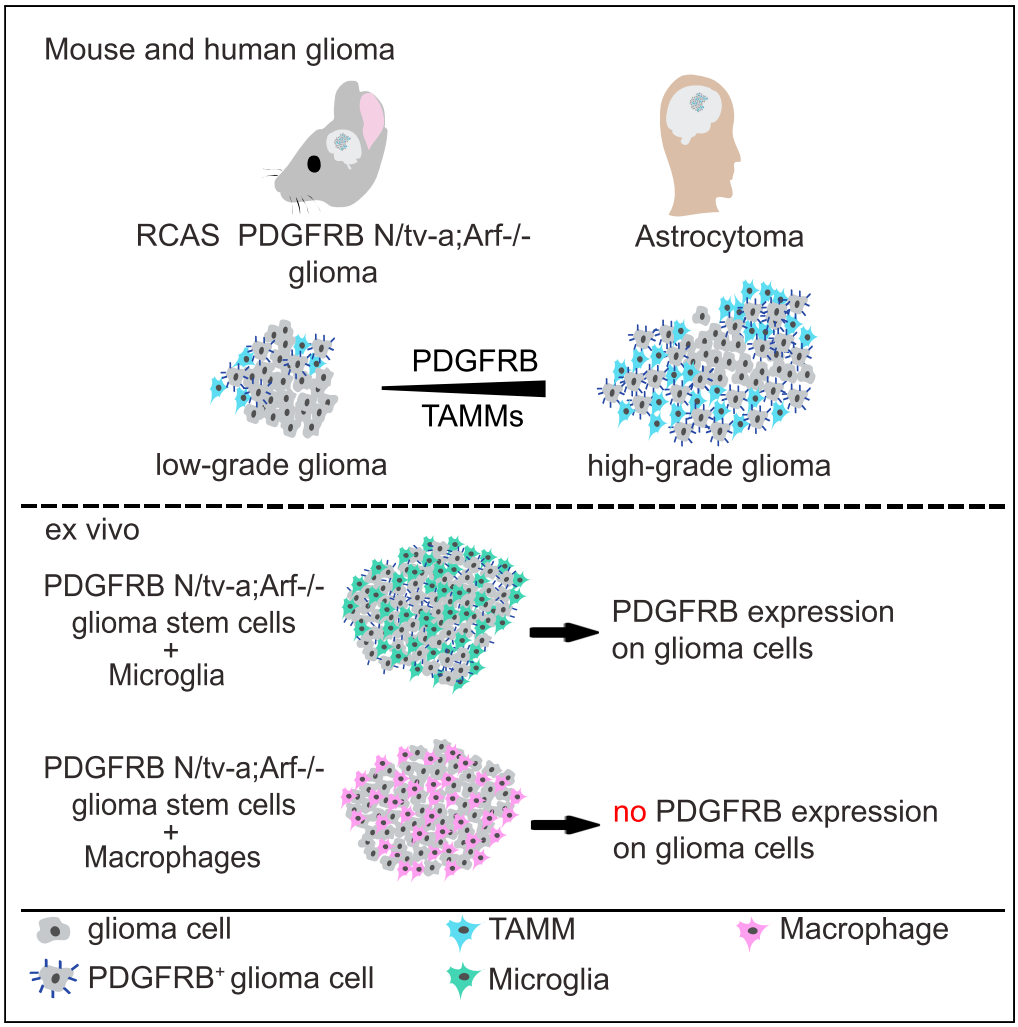


Tatjana Wallmann, Xing-Mei Zhang, Majken Wallerius, ..., Lene Uhrbom, Robert A. Harris, Charlotte Rolny

charlotte.rolny@ki.se

## HIGHLIGHTS

PDGFRB$^+$ glioma cells are in physical contact with IBA1$^+$ TAMMs in mouse and human glioma

Aggregation of PDGFRB$^+$ glioma cells correlated with the accumulation of IBA1$^+$ TAMMs

Microglia but not bone marrow-derived macrophages induced PDGFRB expression *in vitro*

M2-polarized microglia stimulated glioma cell migration dependent on PDGFRB

Wallmann et al., iScience 9, 71–83
November 30, 2018 
https://doi.org/10.1016/j.isci.2018.10.011

iScience

CellPress

Article

# Microglia Induce PDGFRB Expression in Glioma Cells to Enhance Their Migratory Capacity

Tatjana Wallmann,[1] Xing-Mei Zhang,[2] Majken Wallerius,[1] Sara Bolin,[3] Anne-Laure Joly,[4] Caroline Sobocki,[1] Lina Leiss,[1,5,6] Yiwen Jiang,[3,7] Jonas Bergh,[1,8] Eric C. Holland,[9] Per Ø. Enger,[6,10] John Andersson,[4] Fredrik J. Swartling,[3] Hrvoje Miletic,[11,12] Lene Uhrbom,[3] Robert A. Harris,[2] and Charlotte Rolny[1,13,*]

## SUMMARY

**High-grade gliomas (HGGs) are the most aggressive and invasive primary brain tumors. The platelet-derived growth factor (PDGF) signaling pathway drives HGG progression, and enhanced expression of PDGF receptors (PDGFRs) is a well-established aberration in a subset of glioblastomas (GBMs). PDGFRA is expressed in glioma cells, whereas PDGFRB is mostly restricted to the glioma-associated stroma. Here we show that the spatial location of TAMMs correlates with the expansion of a subset of tumor cells that have acquired expression of PDGFRB in both mouse and human low-grade glioma and HCGs. Furthermore, M2-polarized microglia but not bone marrow (BM)-derived macrophages (BMDMs) induced PDGFRB expression in glioma cells and stimulated their migratory capacity. These findings illustrate a heterotypic cross-talk between microglia and glioma cells that may enhance the migratory and invasive capacity of the latter by inducing PDGFRB.**

## INTRODUCTION

Gliomas are the most common primary malignant tumors of the central nervous system (CNS) with different grades of malignancy where grade II is the lowest and grade IV is the highest (Hoshide and Jandial, 2016). The growth pattern of gliomas is characterized by diffuse tumor growth and tumor cell invasion resulting in tumor microsatellites growing far away from the main tumor mass (Hambardzumyan and Bergers, 2015). Diffuse (grade II) and anaplastic (grade III) gliomas are infiltrative neoplasms that most often arise in cerebral hemispheres of adults and include astrocytomas and oligodendrogliomas (Louis et al., 2016). Grade II and III astrocytomas are generally characterized by the IDH1-R132H mutation, whereas oligodendrogliomas are IDH1 mutated and 1p and 19q co-deleted (Hoshide and Jandial, 2016). The latter show better responses to radiochemotherapy and are associated with longer survival than IDH1 wild-type diffuse gliomas or grade IV gliomas denoted glioblastomas (GBMs) (Cancer Genome Atlas Research Network et al., 2015; Eckel-Passow et al., 2015; van den Bent et al., 2013). Conventional therapy for GBMs includes maximal safe surgical resection followed by radiation with concomitant and adjuvant temozolomide treatment that prolongs survival but is not curative (Reifenberger et al., 2016). There is thus an immediate need to develop alternative therapies for GBMs.

There are several cell types in the tumor microenvironment that contribute to glioma malignancy, e.g., astrocytes, endothelial cells, pericytes, and immune cells, including tumor-associated macrophages and microglia (TAMMs) (Quail and Joyce, 2017). Interestingly, almost half of the tumor mass may consist of TAMMs in both murine as well as human gliomas (Hambardzumyan et al., 2016), and the accumulation of TAMMs is associated with poor clinical outcome in gliomas (Chen et al., 2017; Sorensen et al., 2017). In platelet-derived growth factor (PDGFB)-driven glioma the majority of TAMMs is of a pro-tumoral phenotype, and the reprogramming of these TAMMs toward an anti-tumoral phenotype hampers PDGFB-driven glioma growth (Pyonteck et al., 2013; Quail et al., 2016).

PDGFB can bind to both PDGFRA and PDGFRB and is known to play multiple roles in tumor development, both in the tumor cells themselves and within the microenvironment (Kazlauskas, 2017). However, in the RCAS-induced gliomas, it has been postulated that PDGFB drives tumor initiation and progression mainly by activating PDGFRA on nestin$^+$ glial cells (Burton et al., 2001; Holland, 2000; Uhrbom et al., 2002). In concordance, large-scale integrated molecular analyses of GBMs have shown that a subset of these tumors

[1]Karolinska Institutet, Department of Oncology-Pathology, CCK, R8:01, 171 76 Stockholm, Sweden

[2]Karolinska Institutet, Department of Clinical Neuroscience, Karolinska Hospital at Solna, CMM, 171 76 Stockholm, Sweden

[3]Uppsala University, Department of Immunology, Genetics and Pathology, Science for Life Laboratory, Rudbeck Laboratory, 751 85 Uppsala, Sweden

[4]Karolinska Institutet, Department of Medicine, CMM, 171 76 Stockholm, Sweden

[5]Neuro Clinic, Haukeland University Hospital, Bergen, Norway

[6]Oncomatrix Research Lab, University of Bergen, Bergen, Norway

[7]Karolinska Institutet, Department of Medical Biochemistry and Biophysics, 17177 Stockholm, Sweden

[8]Radiumhemmet, Karolinska University Hospital, 171 76 Stockholm, Sweden

[9]Division of Human Biology, Solid Tumor and Translational Research, Fred Hutchinson Cancer Research Center, Seattle, WA 98109, USA

[10]Department of Neurosurgery, Haukeland University Hospital, Bergen, Norway

[11]Department of Pathology, Haukeland University Hospital, Bergen, Norway

*Continued*

are driven by activation of the PDGFRA signaling pathway (Brennan et al., 2013; Verhaak and Valk, 2010), and this has also been confirmed by computational and experimental modeling (Ozawa et al., 2014). The expression of PDGFRB on tumor cells has been less studied, although one study reports that PDGFRB can be expressed in cultured patient-derived GBM cells, particularly in the cancer stem-cell-like population (Kim et al., 2012).

Herein we demonstrated that PDGFRB was expressed on glioma cells (GCs) in mouse and human gliomas in proximity to TAMMs. Both PDGFRB expression on GCs and TAMM accumulation were significantly increased in high-grade gliomas (HGGs) compared with low-grade gliomas (LGGs). Mechanistic studies showed that M2-polarized microglia, but not M2-polarizied bone marrow-derived macrophages (BMDMs), induced GCs to acquire PDGFRB expression and augmented their migratory capacity. In summary, we propose a new mechanism whereby GC migratory behavior may be modulated.

Methods can be found in Transparent Methods in the Supplemental Information.

## RESULTS

### PDGFB-Driven Gliomas in the *N/tv-a;Arf*$^{-/-}$ Mouse Model Display Necrosis, Hypoxia, and Vessel Hyperproliferation Similarly to Human Gliomas

Studies in transgenic mice indicate that gliomas can arise from a range of cell types including neural stem cells, astrocytes, oligodendrocytes, or glial progenitor cells (Jiang et al., 2017; Lindberg et al., 2009). We investigated the role of TAMMs in the *N/tv-a;Arf*$^{-/-}$ mouse model in which the retrovirus will specifically transform glial stem and progenitor cells resulting in glioma development between 1 to 3 months (Karrlander et al., 2009; Tchougounova et al., 2007). According to histopathological characteristics (evaluated by neuropathologist H. Miletic) the tumors were divided into human grade II-, grade III- and grade IV-like gliomas, where grade IV-like gliomas displayed necrotic areas (Figure 1A). GCs and glioblastoma stem cells (GSCs) in particular express OLIG2 (Lu et al., 2016), which in the normal brain is restricted to oligodendroglial cells and their progenitors (Mitew et al., 2014). Gliomas that display OLIG2$^{+}$GCs that have acquired the expression of the glial fibrillary acidic protein (GFAP), which defines differentiated astrocytes, are generally classified as astrocytomas (Moeton et al., 2014), whereas OLIG2$^{+}$GCs that are negative for GFAP are typically classified as oligodendrogliomas that can never develop into a grade IV glioma (Hoshide and Jandial, 2016). Importantly, all the PDGFB-driven grade II-, grade III-, and grade IV-like gliomas displayed OLIG2$^{+}$GFAP$^{+}$GCs (Figure 1B), indicating that these tumors are low- or high-grade astrocytomas rather than oligodendrogliomas (Skalli et al., 2013).

Tumor necrosis is associated with poorly perfused abnormal vessels with proliferative endothelial cells, resulting in an inadequate supply of the tumor with oxygen and nutrients (Jain, 2014). Increased vessel area, decreased vessel perfusion, and hypoxia generally indicate vessel abnormalization that correlates with tumor malignancy (Mazzone et al., 2009; Rolny et al., 2011). Hence, we next performed morphometric analysis for CD31 (endothelial cell marker) and fluorescein isothiocyanate-conjugated lectin, which detects perfused vessels (Figure 1C), or pimonidazole hydrochloride staining, which identifies hypoxic areas (Figure 2A). Both vessel area (Figures 1C and 1D) and vessel density (Figures 1C and 1E) were evidently increased between grade II- and grade III-like gliomas, and between grade II- and grade IV-like gliomas. Consistently, vessel perfusion (Figures 1C, 1F, and 1G) was markedly decreased, whereas hypoxia (Figures 2A and 2B) was increased in grade III- and grade IV-like gliomas compared with grade II-like gliomas. These features suggested that most of the vessels in the grade II-like gliomas are co-opted, non-angiogenic vessels (Holash et al., 1999). In corroboration, endothelial cells in grade II-like gliomas displayed significantly less proliferation compared with grade III- and grade IV-like gliomas as visualized by staining of tumor sections for podocalyxin and Ki67 (Figures 2C and 2D).

Displacement of pericytes covering the tumor vessels is yet another hallmark of vessel abnormalization and dysfunctionality (Baluk et al., 2003; Mazzone et al., 2009). Tumor sections were therefore stained for OLIG2, CD31, and the pericyte marker α-smooth muscle actin (α-SMA). The accumulation of α-SMA$^{+}$ cells was profoundly increased with the degree of malignancy (Figures 2E and 2F). Surprisingly, the majority of the α-SMA$^{+}$ cells were not found in conjugation with perfused vessels (Figures 2G and 2H) and were instead in close association with IBA1$^{+}$ TAMMs (Figure 2I).

[12]Department of Biomedicine, University of Bergen, Bergen, Norway

[13]Lead Contact

*Correspondence: charlotte.rolny@ki.se

https://doi.org/10.1016/j.isci.2018.10.011

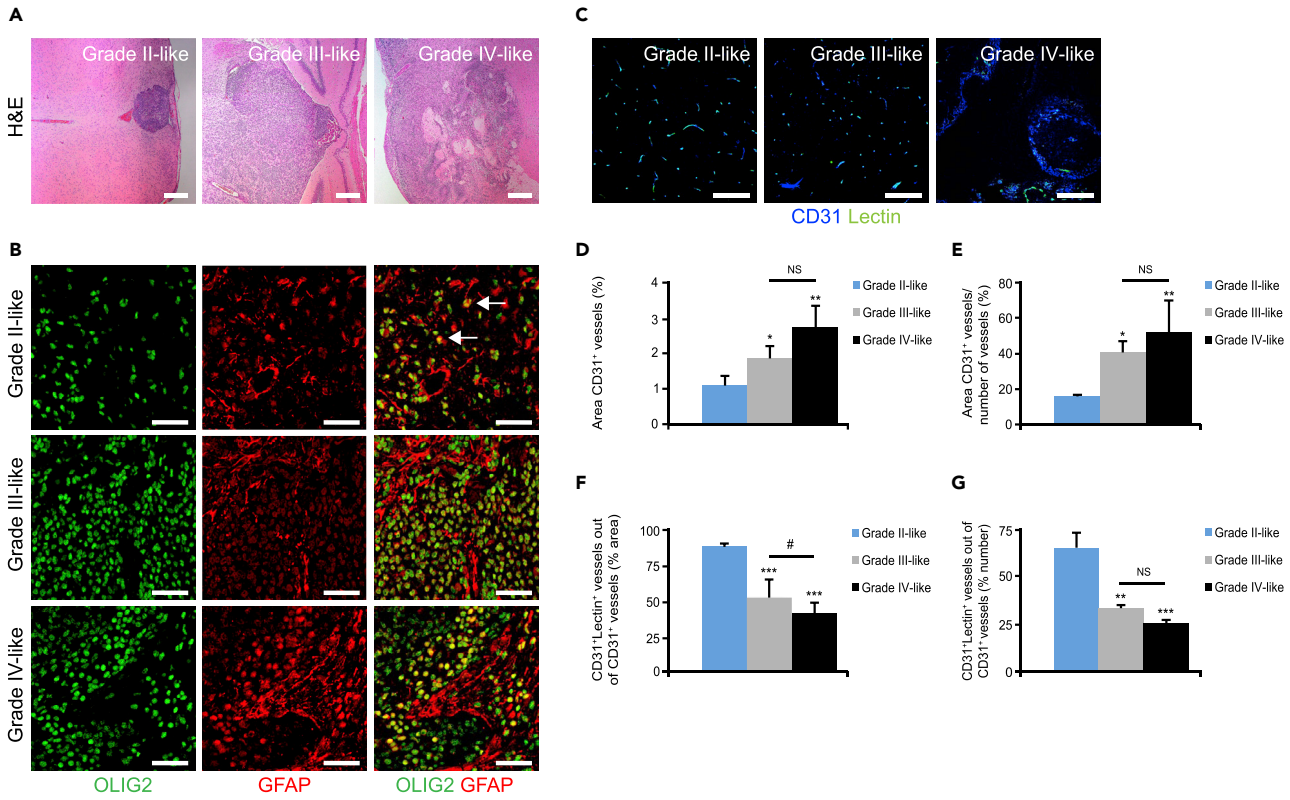


**Figure 1. PDGFB-Driven Gliomas in the *N/tv-a;Arf*$^{-/-}$ Mouse Model Display Necrosis and Decreased Vessel Perfusion**

(A) Images display tumor sections immunostained with H&E. Scale bars, 200 μm.

(B) Glioma sections were immunostained for OLIG2 (green) and GFAP (red). Scale bars, 50 μm.

(C–G) (C) Images display tumors perfused with fluorescein isothiocyanate-conjugated lectin (green) and immunostained for the endothelial marker CD31 (blue). Graphs display (D) vessel area, (E) vessel density, (F) area of perfused vessels, and (G) % number of perfused vessels. (n = 3–5). Scale bars, 100 μm. Statistical analysis: one-way ANOVA was used; *$p < 0.05$, **$p < 0.01$, ***$p < 0.001$; * indicates significance compared with grade II-like tumors; $^{\#}p < 0.05$; $^{\#}$ indicates significance between grade III- and grade IV-like tumors.

## Glioma Cells Express Pericyte Markers in Mouse and Human Gliomas

To investigate whether the α-SMA$^+$ cells were indeed bona fide pericytes, grade IV-like gliomas were stained for the pericyte markers PDGFRB and NG2 (that also stains oligodendrocyte progenitor cells). The majority of the α-SMA$^+$ cells that appeared in sheets did indeed express PDGFRB (Figure 3A) and NG2 (Figure 3B), and a portion of these cells also expressed the mesenchymal marker CD44 (Figure 3C), but were negative for GC and GSC markers including SOX2 (Figure 3D), OLIG2 (Figure 3E), and GFAP (Figure 3F). Intriguingly, α-SMA$^+$ cells that appeared as round cells did indeed express GC and GSC markers including SOX2 (Figure 3D), OLIG2 (Figure 3E), and GFAP (Figure 3F). Importantly, these α-SMA$^+$ cells also expressed the hemagglutinin (HA) tag, which can only be expressed by the initial RCAS-infected nestin-expressing glial cells (Figure 3G). The round α-SMA$^+$SOX2$^+$, α-SMA$^+$OLIG2$^+$, α-SMA$^+$GFAP$^+$, and α-SMA$^+$HA$^+$ cells accounted for ~20% of the total α-SMA population in grade IV-like gliomas (Figure 3H).

## Spatial Location of αSMA$^+$PDGFRB$^+$GCs in Mouse and Human Gliomas

It has previously been proposed that GSCs can give rise to perivascular pericytes (Cheng et al., 2013) and are located in the vicinity of tumor vessels. However, here we find that α-SMA$^+$ OLIG2$^+$ (Figure 4A), α-SMA$^+$SOX2$^+$ (Figure 4B), and α-SMA$^+$PDGFRB$^+$ cells (Figure 4C) are scattered throughout the tumor mass and are not located perivascularly. Our observation that α-SMA$^+$GCs rarely attached to vessels led us to investigate if these α-SMA$^+$GCs were associated with other types of stromal cells such as TAMMs that accumulate in HGGs (Pyonteck et al., 2013; Quail et al., 2016). Indeed, IBA1$^+$ TAMMs were closely associated with α-SMA$^+$HA$^+$ (Figure 4D) and PDGFRB$^+$HA$^+$ (Figure 4E) cells in mouse HGGs. Of note,

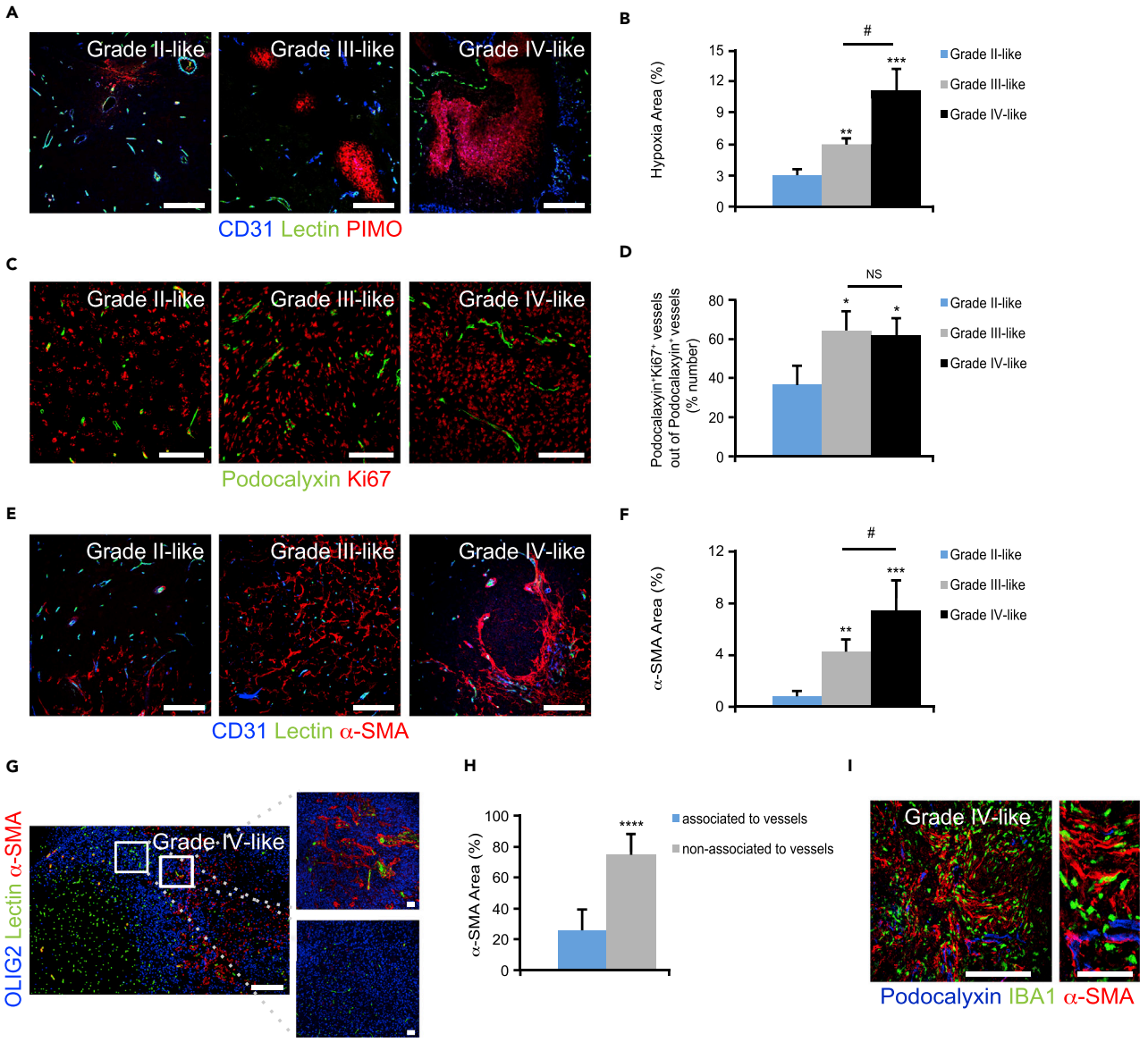


**Figure 2. PDGFB-Driven Gliomas in the *N/tv-a;Arf*$^{-/-}$ Mouse Model Display Hypoxia and Vessel Hyperproliferation**

(A and B) (A) Glioma sections were immunostained for CD31 (blue), fluorescein isothiocyanate (FITC)-conjugated lectin (green), and the hypoxic marker pimonidazole (PIMO; red). (B) Graph shows morphometric analysis of hypoxic areas (n = 3–5). Scale bars, 100 μm.

(C and D) (C) Glioma sections were immunostained for podocalyxin (green) and Ki67 (red). (D) Graph depicts quantification of podocalyxin$^{+}$Ki67$^{+}$ vessels (n = 3). Scale bars, 100 μm.

(E and F) (E) Glioma sections were immunostained for CD31 (blue), FITC-conjugated lectin (green), and the pericyte marker α-SMA (red). (F) Graph displays quantification of α-SMA (n = 3–5). Scale bars, 100 μm.

(G and H) (G) Glioma sections were immunostained for OLIG2 (blue), FITC-conjugated lectin (green), and α-SMA (red). (H) Graph shows analysis of α-SMA$^{+}$ sheets associated with vessels. Scale bars, 100 (left panel) and 50 (right panel) μm.

(I) Glioma sections were immunostained for podocalyxin (blue), microglia marker IBA1 (green), and α-SMA (red). Scale bars, 100 (left panel) and 50 μm (right panel).

Statistical analysis: one-way ANOVA (A–F) and student's t test (G and H) were used: *$p < 0.05$, **$p < 0.01$, ***$p < 0.001$, ****$p < 0.0001$; * indicates significance (A–F) compared with grade II-like tumors and (H) between α-SMA$^{+}$ sheets associated and non-associated with vessels; $^{\#}p < 0.05$; $^{\#}$ indicates significance between grade III- and grade IV-like tumors.

α-SMA$^{+}$IDH1-R132H$^{+}$ cells were also in close proximity to IBA1$^{+}$ TAMMs in human HGGs (Figure S1). We then speculated that PDGFRB$^{+}$GCs might correlate to the accumulation of TAMMs in mouse and human gliomas. Indeed, PDGFRB$^{+}$HA$^{+}$ (Figures 5A–5E), PDGFRB$^{+}$IDH1-R132H$^{+}$, and PDGFRB$^{+}$GFAP$^{+}$ cells

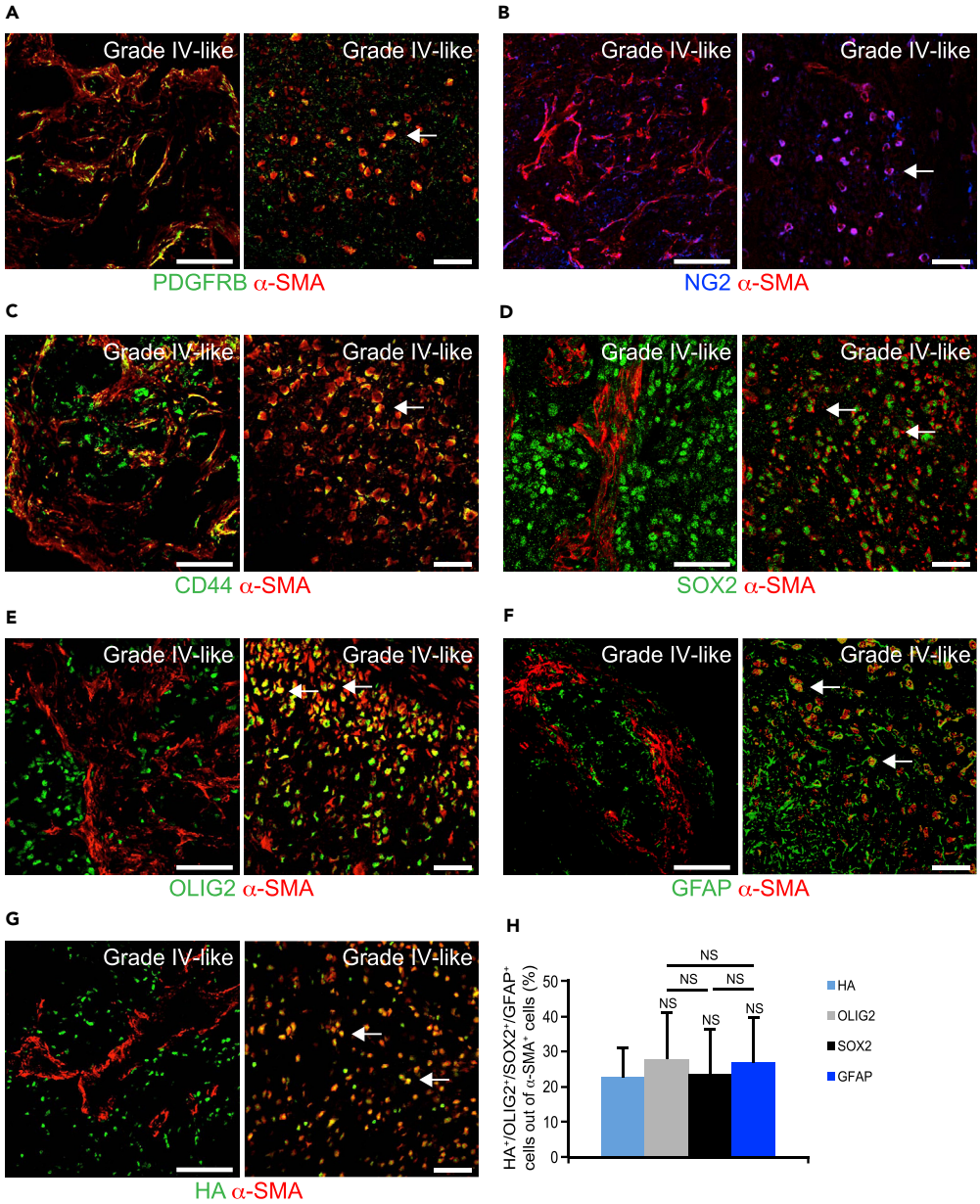


**Figure 3. Glioma Cells Express Pericyte Markers in Mouse Gliomas**

(A–H) Mouse glioma sections were immunostained for (A) α-SMA (red) and the pericyte marker PDGFRB (green), (B) α-SMA (red) and the pericyte and oligodendrocyte marker NG2 (blue), (C) α-SMA (red) and the mesenchymal and stem cell marker CD44 (green), (D) α-SMA (red) and the GSC marker SOX2 (green), (E) α-SMA (red) and the oligodendrocyte marker OLIG2 (green), (F) α-SMA (red) and the astrocyte marker GFAP (green), and (G) α-SMA (red) and the HA tag expressed by PDGF-B-transformed cells (green). Left panels show α-SMA$^+$ sheets, whereas right panels display round α-SMA$^+$ cells. Scale bars, 100 (left panel) and 50 (right panel) μm. (H) Graph displays quantification of HA$^+$, OLIG2$^+$, SOX2$^+$, and GFAP$^+$ cells out of α-SMA$^+$ cells (n = 3).

Statistical analysis: one-way ANOVA was used.

correlated to TAMM accumulation (Figures 5F–5J). In fact, ~70% of PDGFRB$^+$GCs in grade III- and grade IV-like mouse gliomas (Figure 5E) and human GBMs (Figure 5J) were in physical contact with IBA1$^+$ TAMMs. It has recently been revealed that the transcription factor Sall1 is preferentially expressed by microglia and not macrophages (Buttgereit et al., 2016). In fact, the majority of IBA1$^+$ TAMMs expressed Sall1 (Figure S2A) and not CD49d (Figure S2B), which is preferentially expressed by macrophages, indicating that these cells

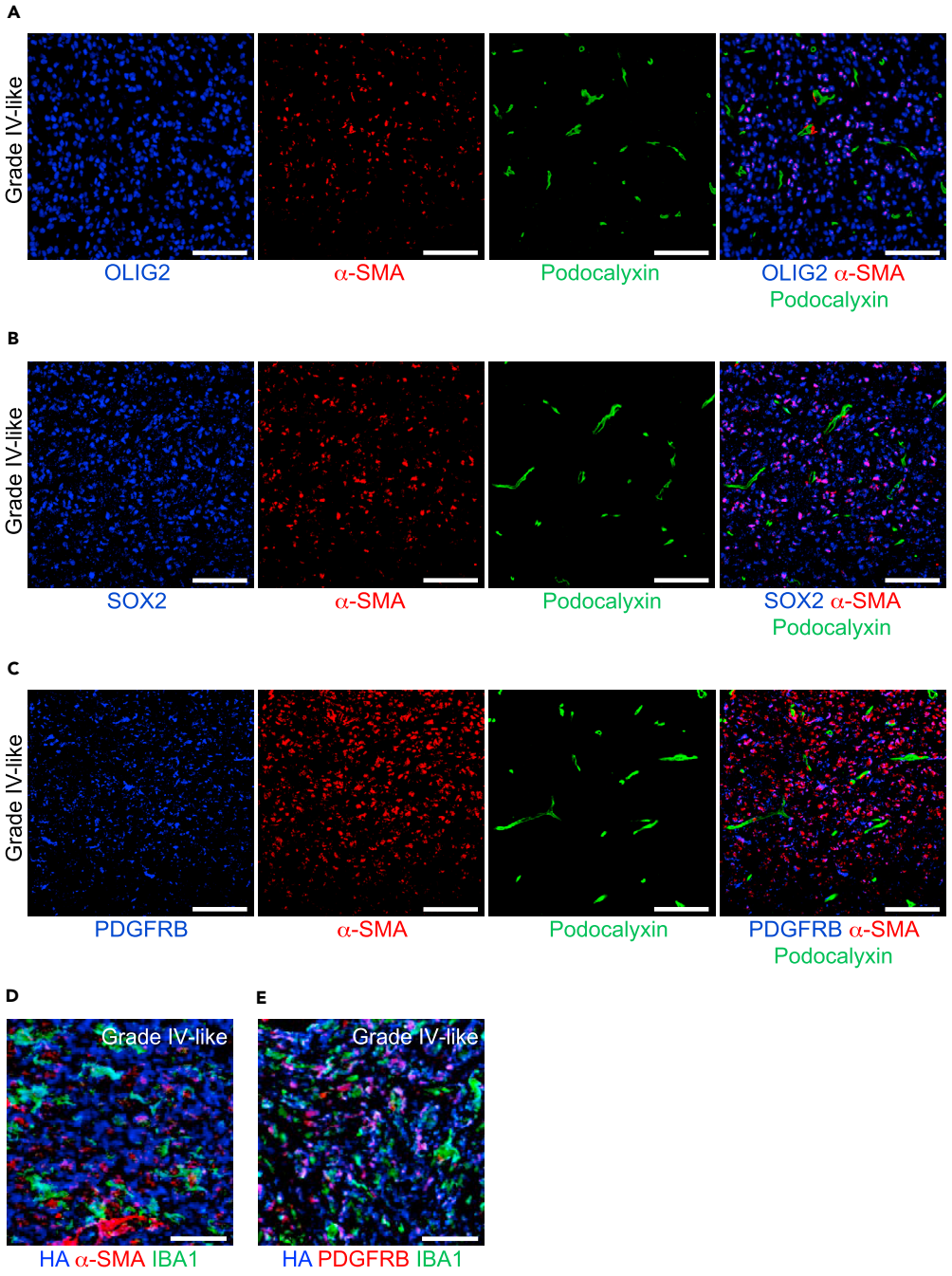


**Figure 4. Spatial Location of α-SMA$^+$SOX2$^+$, α-SMA$^+$OLIG2$^+$, and α-SMA$^+$PDGFRB$^+$ GCs in Mouse Gliomas**

(A–C) Mouse glioma sections were immunostained for (A) OLIG2 (blue), α-SMA (red), and podocalyxin (green); (B) SOX2 (blue), α-SMA (red), and podocalyxin (green); and (C) PDGFRB (blue), α-SMA (red), and podocalyxin (green). Scale bars, 100 μm.

(D) Mouse grade IV-like glioma sections were immunostained for HA tag (expressed by PDGFB-transformed cells; blue), α-SMA (red), and IBA1 (green). Scale bars, 50 μm.

(E) Mouse grade IV-like glioma sections were immunostained for HA tag (blue), PDGFRB (red), and IBA1 (green). Scale bars, 50 μm.

See also Figure S1.

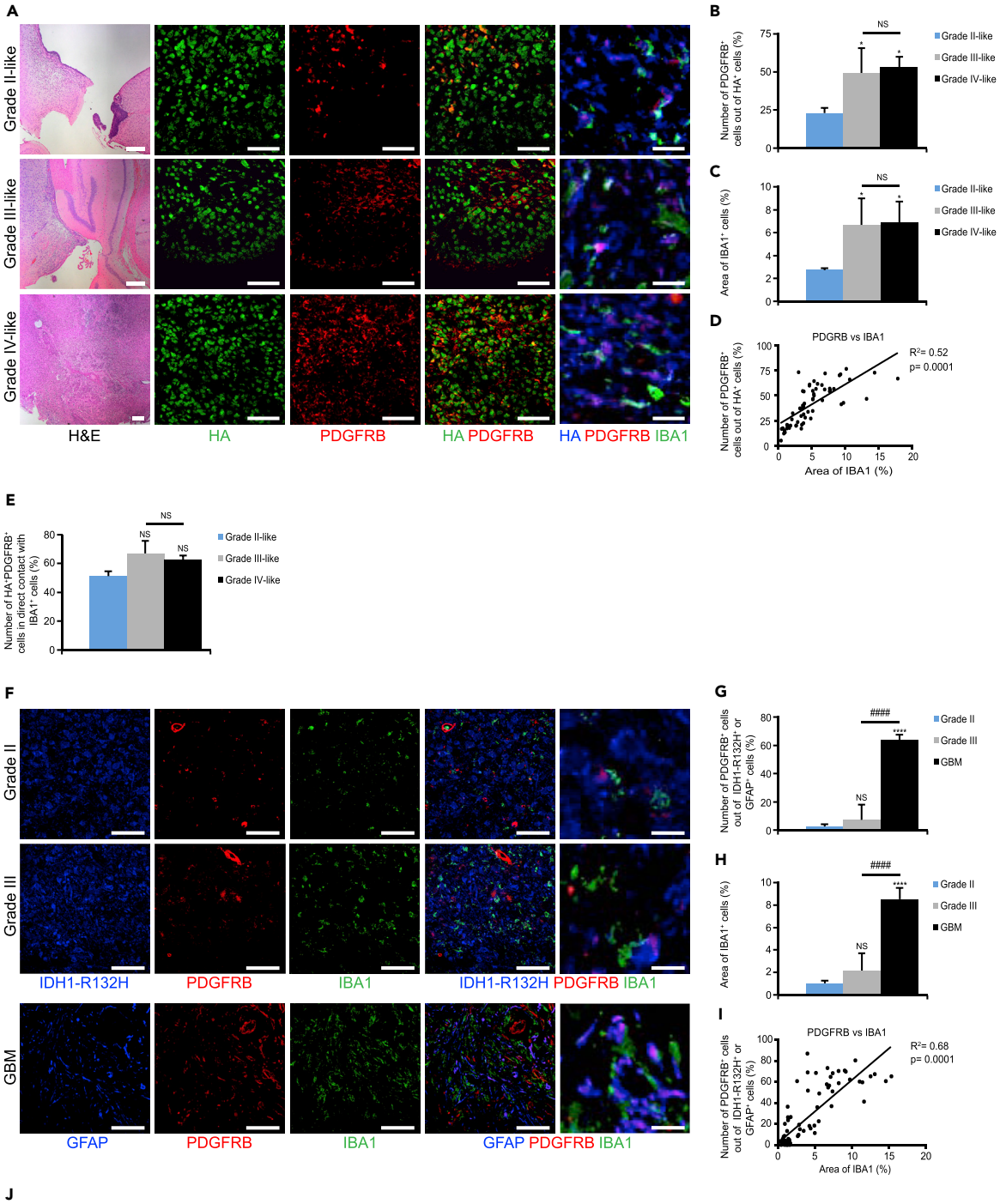
A
Grade II-like
Grade III-like
Grade IV-like
H&E
HA
PDGFRB
HA PDGFRB
HA PDGFRB IBA1
B
Number of PDGFRB+ cells out of HA+ cells (%)
NS
Grade II-like
Grade III-like
Grade IV-like
C
Area of IBA1+ cells (%)
NS
Grade II-like
Grade III-like
Grade IV-like
D
PDGRB vs IBA1
R²= 0.52
p= 0.0001
Number of PDGFRB+ cells out of HA+ cells (%)
Area of IBA1 (%)
E
Number of HA+PDGFRB+ cells in direct contact with IBA1+ cells (%)
NS
NS
NS
Grade II-like
Grade III-like
Grade IV-like
F
Grade II
Grade III
GBM
IDH1-R132H
PDGFRB
IBA1
IDH1-R132H PDGFRB IBA1
GFAP
PDGFRB
IBA1
GFAP PDGFRB IBA1
G
Number of PDGFRB+ cells out of IDH1-R132H+ or GFAP+ cells (%)
####
****
NS
Grade II
Grade III
GBM
H
Area of IBA1+ cells (%)
####
****
NS
Grade II
Grade III
GBM
I
PDGFRB vs IBA1
R²= 0.68
p= 0.0001
Number of PDGFRB+ cells out of IDH1-R132H+ or GFAP+ cells (%)
Area of IBA1 (%)
J
Number of IDH1-R132H+PDGFRB+ or GFAP+PDGFRB+ cells in direct contact with IBA1+ cells (%)
###
***
NS
Grade II
Grade III
GBM

**Figure 5. Glioma Cells Express PDGFRB and Correlate with IBA1$^+$ TAMMs in Mouse and Human Gliomas**

(A–E) (A) Mouse glioma sections were immunostained for H&E, HA tag (green/blue), PDGFRB (red), and IBA1 (green). Graphs display (B) number of PDGFRB$^+$HA$^+$ cells out of HA$^+$ cells, (C) area of IBA1$^+$ cells, (D) Pearson's correlation between PDGFRB$^+$ cells versus area of IBA1, and (E) number of PDGFRB$^+$HA$^+$ cells in contact with IBA1$^+$ cells (n = 3–5). Scale bars 200 (left panel), 50 (middle panel), and 20 (far right panel) μm.

(F–J) (F) Human glioma sections were immunostained for IDH1-R132H or GFAP (blue), PDGFRB (red), and IBA1 (green). Graphs depict (G) number of PDGFRB$^+$IDH1-R132H$^+$ cells or PDGFRB$^+$GFAP$^+$ cells out of IDH1-R132H$^+$ or GFAP$^+$ cells, (H) area of IBA1$^+$ cells, (I) Pearson's correlation between PDGFRB$^+$ cells versus area of IBA1, and (J) number of PDGFRB$^+$IDH1-R132H$^+$ or PDGFRB$^+$GFAP$^+$ cells in contact with IBA1$^+$ cells (n = 5–6). Scale bars, 50 (left panel) and 20 (far right panel) μm.

Statistical analysis: one-way ANOVA (B, C, E, G, H, and J) and Pearson's correlation (D and I) were used: *$p < 0.05$, ***$p < 0.001$, ****$p < 0.0001$; * indicates significance compared with grade II-like tumors; $^{\#\#\#}p < 0.001$, $^{\#\#\#\#}p < 0.0001$; $^{\#}$ indicates significance between grade III- and grade IV-like tumors. See also Figure S2.

were microglia and not macrophages. In summary, the spatial location of TAMM accumulation strongly correlated with α-SMA$^+$ and PDGFRB$^+$GCs.

## TAMMs Induce Mouse Glioma Cells to Express PDGFRB

We hypothesized that pro-tumoral TAMMs could drive tumor cells to express *pdgfrb* due to their spatial localization. Thus, microglia derived from adult mice polarized to an M1-phenotype (lipopolysaccharide [LPS] and interferon [IFN]-γ) or an M2 phenotype (interleukin [IL]-4, IL-10, and transforming growth factor [TGF]-β) *in vitro* were co-cultured with GFP$^+$GSCs derived from grade IV-like PDGFB-induced tumors in *N/tv-a;Arf*$^{-/-}$ mice. As expected, qPCR analysis showed that M1-polarized microglia displayed high gene expression levels of chemokine (C-X-C motif) ligand (*cxcl9*, *cxcl10*, *cxcl11*, *il-6*, and *il-1β*, whereas M2-polarized microglia showed high expression levels of *arginase 1*, *mrc1*, and *ym1* (Figure 6A). Interestingly, GFP$^+$GSCs flow sorted from the co-culture system displayed induced levels of *pdgfrb* (Figure 6B) and increased levels of *α-sma* transcription levels (30-fold; Figure 6C) in the presence of M2-polarized microglia. Surprisingly, co-culture with M1-polarized microglia also induced *pdgfrb* expression (Figure 6B) and increased *α-sma* levels (Figure 6C), but significantly less compared with M2 microglia. Importantly, basal expression of *pdgfrb* was undetectable. Notably, *pdgfra* was not affected by either M1- or M2-polarized microglia (Figure 6D).

As GCs have been shown to express different tyrosine kinases, we next examined if M2-polarized microglia could alter the expression of a variety of tyrosine kinase receptors, including epidermal growth factor receptor (*egfr*), fibroblast growth factor receptor (*fgfr*), hepatocyte growth factor receptor (*hgfr*), or insulin-like growth factor-1 receptor (*igf-1r*). In fact, M1- and M2-polarized microglia did not affect the expression of *fgfr*, *igf-1r* (Figure 6E), *or hgfr* (Figure 6F). Even though M1- and M2-polarized microglia could induce *egfr* expression in GCs, the expression levels were about 100-fold less compared with that of *pdgfrb* (Figure 6F). We further explored if the expression of *pdgfrb* in GCs could also be modulated by microglia-secreted factors. GCs were thus cultured with control medium or conditioned medium from M1- or M2-polarized microglia. Interestingly, neither *pdgfrb* nor *α-sma* expression could be either induced or increased, respectively, in the presence of conditioned medium from either M1- or M2-polarized microglia (Figure 6G).

Recent studies report that microglia are not only ontologically different from BMDMs (Gomez Perdiguero et al., 2015) but also exhibit distinct activation states based on diverse gene and surface marker expression, implying different functions compared with BMDMs (Bowman et al., 2016). We therefore investigated if BMDMs were capable of inducing the expression of *pdgfrb* in GCs by co-culturing GFP$^+$GSCs with either M1-BMDMs (treated with LPS and IFN-γ) or M2-polarized BMDMs (treated with IL-4, IL-10, and TGF-β). These BMDMs displayed the same repertoire of cytokines as M1- and M2-polarized microglia. Surprisingly, neither M1- nor M2-polarized BMDMs could induce *pdgfrb* or increase the *α-sma* expression in GCs (Figure 6H). Intriguingly, preconditioning of BMDMs with medium from primary microglia culture did not induce *pdgfrb* or increase *α-sma* expression in GCs either (data not shown).

In summary, only cell-to-cell contact with microglia could induce *pdgfrb* expression in GCs. We further explored if M1- or M2-polarized microglial cell-to-cell contact with GSCs could further alter their expression of glial, stem, and progenitor cell markers. Surprisingly, most glial stem cell and progenitor cell markers including *nestin*, *olig2*, *sox2* (Figure 6I), *ng2*, and *hes1* (Figure 6J) were not further modified by the presence of M1- or M2-polarized microglia. Interestingly, the marker for late oligodendrocyte precursor cells *cnp* (Lindberg et al., 2009) (Figure 6J) was markedly decreased by both M1- and M2-polarized microglia, whereas the astrocytoma marker *gfap* (Figure 6K) was markedly increased by M2-polarized microglia. These findings indicate that regardless of the polarization state, microglia did not affect an overall increase in stem and progenitor cell markers.

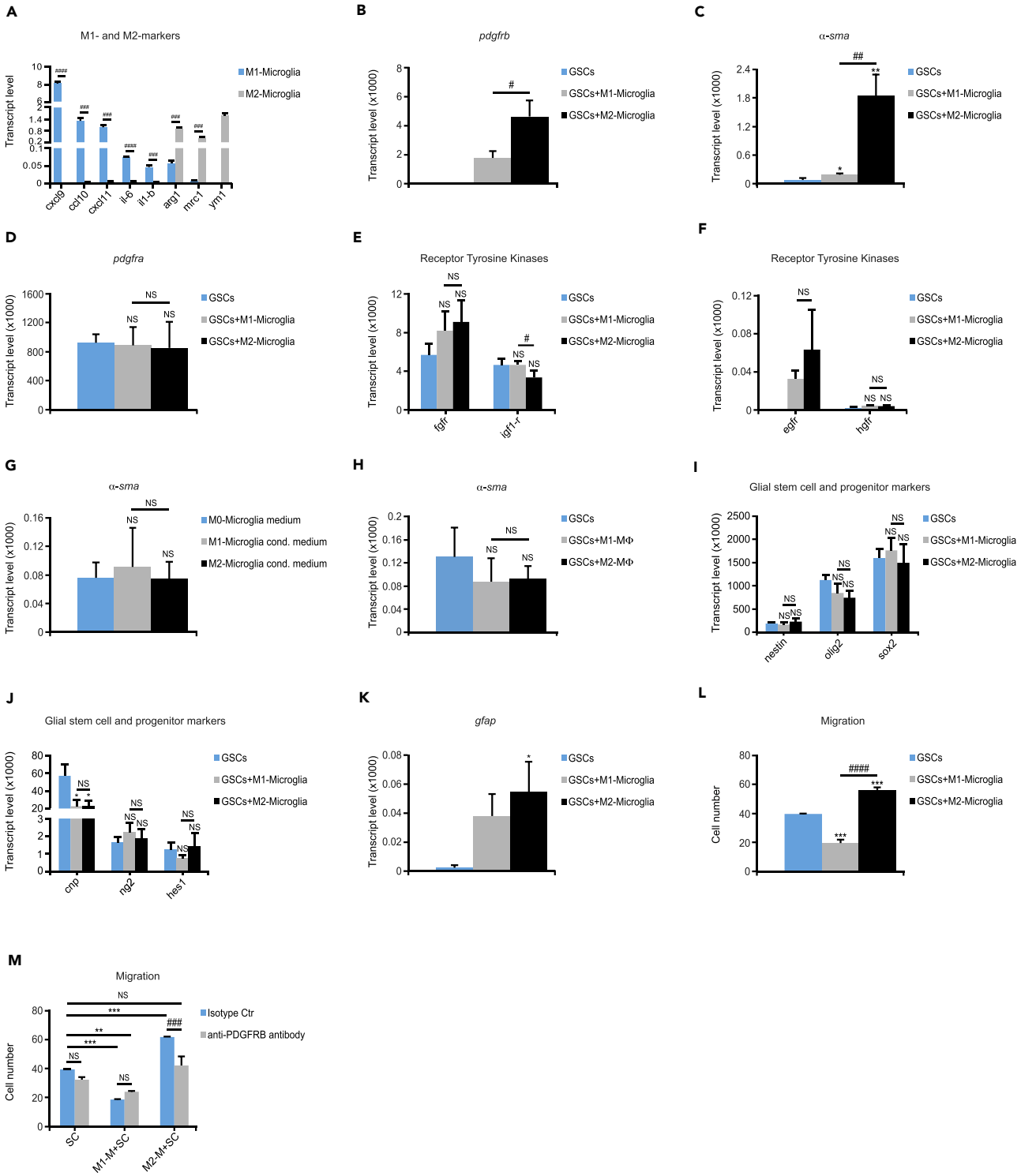


**Figure 6. TAMMs Induce Mouse Glioma Cells to Express PDGFRB**

(A) Microglia were polarized to either an M1 or M2 phenotype. Graph shows gene expression levels of *cxcl9*, *cxcl10*, *cxcl11*, *il-6*, *il-1b*, *arginase1*, *mrc1*, *and ym1* analyzed by qRT-PCR (n = 3).

(B–F) GFP$^+$GSCs were co-cultured with M1- or M2-polarized microglia. Graphs depict qRT-PCR analysis of gene expression levels of flow-sorted tumor cells for (B) *pdgfrb*, (C) *α-sma*, (D) *pdgfra*, (E) *fgfr* and *igf-1r*, and (F) *egfr* and *hgfr* (n = 3).

**Figure 6. *Continued***

(G) GFP$^+$GSCs were cultured with M0 (not polarized)-, M1- or M2-like microglia conditioned media. Graph displays gene expression levels for *α-sma* quantified by quantitative RT-PCR (n = 3).

(H) GFP$^+$GSCs were co-cultured with M1- or M2-polarized BMDMs. Graph shows qRT-PCR analysis of gene expression levels of flow-sorted tumor cells for *α-sma* (n = 3).

(I–K) GFP$^+$GSCs were co-cultured with M1- or M2-polarized microglia. Graphs depict quantitative RT-PCR analysis of gene expression levels of flow-sorted tumor cells for (I) *nestin*, *olig2,* and *sox2;* (J) *cnp, ng2,* and *hes1;* and (K) *gfap* (n = 3).

(L and M) GFP$^+$GSCs were co-cultured with M1- or M2-polarized microglia, and migrated tumor cells were stained for the OLIG2 marker. Graphs display (L) migrated tumor cells (n = 3) and (M) migrated tumor cells with isotype control or neutralizing PDGFRB antibody (n = 3).

Statistical analysis: Student's t test (A) and one-way ANOVA (B–M) were used: *$p < 0.05$, **$p < 0.01$, ***$p < 0.001$; * indicates significance (B–L) compared with tumor cells alone, and (M) compared with tumor cells without PDGFRB blockage; $^{\#}p < 0.05$, $^{\#\#}p < 0.01$, $^{\#\#\#}p < 0.001$, $^{\#\#\#\#}p < 0.0001$; # indicates significance between (A) M1-like and M2-like microglia and (B–L) tumor cells co-cultured with M1 microglia compared with M2 microglia and (M) tumor cells co-cultured with M2-like microglia without PDGFRB blockage compared with PDGFRB blockage. All data represent one out of three independent experiments and are presented as the mean +SD. See also Table S1.

In agreement with the notion that the PDGFRB signaling pathway is a key modulator in regulating cell migration (Kazlauskas, 2017), we explored if M1- and M2-polarized microglia could affect the migration of cultured GCs. GFP$^+$GSCs were therefore co-cultured with M1- or M2-polarized microglia before subjecting them to a Boyden chamber. Intriguingly, M2-polarized microglia fueled the migratory capacity of GCs (Figure 6L), whereas M1-polarized microglia significantly suppressed GC migration (Figure 6L). Blocking PDGFRB revoked the effect of M2-polarized microglia on tumor cell migration but had no effect on the M1-polarized-microglia-mediated inhibition of GC migration (Figure 6M). In summary, M2-polarized-microglia-stimulated migration of GCs was mediated by PDGFRB.

## DISCUSSION

Herein we show that the presence of PDGFRB$^+$GCs and α-SMA$^+$GCs in mouse and human HGGs was tightly interlinked with the number of and physical proximity to TAMMs. Accordingly, both mouse and human LGGs displayed low frequency of TAMMs and PDGFRB$^+$GCs, whereas grade III- and grade IV-like murine gliomas and human GBMs displayed high frequency of TAMMs and PDGFRB$^+$GCs. Human grade III astrocytomas displayed a large heterogeneity in the accumulation of TAMMs and, therefore the frequency of PDGFRB$^+$GCs also varied accordingly. TAMMs consist of a mixed population including tissue-resident microglia and macrophages that are ontogenetically different (Bowman et al., 2016). Microglia develop from embryonic yolk sac progenitor cells (Gomez Perdiguero et al., 2015) and only populate the brain during development. Thus, during adulthood microglia are maintained through survival and local proliferation (Ajami et al., 2007; Gomez Perdiguero et al., 2015). Conversely, macrophages develop from hematopoietic precursors during embryonic development and establish stable resident populations in extracranial tissues (Goldmann et al., 2016). The macrophages that populate GBMs are recruited to the tumor from the bone marrow (Quail and Joyce, 2017). The different origins of BMDMs and tissue-resident microglia result from distinct transcriptional and chromatin states, and the expression of markers in these cell populations may reflect different functions of tissue-resident microglia and BMDMs in GBMs (Bowman et al., 2016). Macrophages preferentially express CD49d (Bowman et al., 2016), whereas microglia show expression of Sall1 (Buttgereit et al., 2016). Interestingly, the majority of IBA1$^+$ cells expressed Sall1 in mouse gliomas, pointing out that these cells were microglia and not macrophages. The induced and increased expression of PDGFRB and α-SMA in GCs, respectively, was ascribed to cell-to-cell contact with M2-polarized microglia but not with M2-polarized BMDMs.

Interestingly, *in vitro* co-culture of GSCs and M1- or M2-polarized microglia did not further augment stem cell marker expression, but instead downregulated oligodendrocyte progenitor marker *cnp*, whereas the astrocytoma marker *gfap* was markedly increased by M2-polarized microglia. GFAP is the hallmark in intermediate filaments and has been implicated in regulating the migratory capacity of GCs (Moeton et al., 2014). Hence, M2-polarized microglia induce not only high expression of PDGFRB but also high expression of GFAP. This in concert could possibly promote tumor cel0l migratory capacity. We speculate that microglia-GC-to-cell contact regulates PDGFRB transcription affecting any of the known transcription factors (NF-Y or Sp1) that promote PDGFRB transcription (Ishisaki et al., 1997; Molander et al., 2001). The underlying mechanisms whereby PDGFRB transcription is regulated by microglia deserve future investigations but lie outside the scope of the present investigation. In summary, these findings indicate that microglia and BMDM may affect GC behavior differently and deserve further investigation.

### Limitations of the Study

Currently, evidence is increasing about differences in function between microglia and macrophages. In concordance with our study, we show that microglia but not macrophages induce PDGFRB expression in GCs and thereby increase their migratory capacity. However, due to limitations of antibody combinations, it was not possible to use the two markers Sall1 and CD49d in the same immunofluorescence staining to distinguish between microglia and macrophages that are in direct contact with PDGFRB-expressing GCs. Hence elaborate lineage-tracing animal experiments are further needed to establish the differential role of macrophages and microglia in driving PDGFRB expression *in vivo*.

## METHODS

All methods can be found in the accompanying Transparent Methods supplemental file.

## SUPPLEMENTAL INFORMATION

Supplemental Information includes Transparent Methods, two figures, and one table and can be found with this article online at https://doi.org/10.1016/j.isci.2018.10.011.

## ACKNOWLEDGMENTS

The authors thank for technical support of histology lab service the CCK core facility. This study was supported by the Swedish Cancer Society (2016/825), Swedish Cancer Society (CAN 2016/791), Swedish Scientific Council (2013-5982), and Wallenberg Foundation to C.R. and T.W. was supported by KI PhD Foundation. X.-M.Z. was supported by Swedish Childhood Cancer Foundation (NCP2015-0064, NC2014-0046, PR2014-0154). Swedish Cancer Society (CAN 2016/791) and the Wallenberg foundation to J.B.

## AUTHOR CONTRIBUTIONS

Methodology, T.W. and C.R.; Investigation, T.W., X-M.Z., M.W., S.B., A-L. J., C.S., and H.M.; Resources, Y.J., J.B., E.C.H., P.Ø .E., J.A., F.J.S., L.U., and R.A.H and E.C.H and L.W.; Writing – Original Draft, T.W., M.W., and C.R.; Writing – Review & Editing, T.W., X.-M.Z., M.W., A-L.J., H.M., J.A., F.J.S., L.U., R.A.H., and C.R.; Supervision, C.R.; Project Administration, C.R.

## DECLARATION OF INTERESTS

The authors declare no competing interests.

Received: April 27, 2018
Revised: June 22, 2018
Accepted: October 10, 2018
Published: November 30, 2018

## SUPPORTING CITATIONS

Criscuoli et al. (2005); Dreher et al. (2006); Holland and Varmus (1998); Jiang et al. (2011); Wallerius et al. (2016); Zhang et al. (2014).

## REFERENCES

Ajami, B., Bennett, J.L., Krieger, C., Tetzlaff, W., and Rossi, F.M. (2007). Local self-renewal can sustain CNS microglia maintenance and function throughout adult life. Nat. Neurosci. *10*, 1538–1543.

Baluk, P., Morikawa, S., Haskell, A., Mancuso, M., and McDonald, D.M. (2003). Abnormalities of basement membrane on blood vessels and endothelial sprouts in tumors. Am. J. Pathol. *163*, 1801–1815.

Bowman, R.L., Klemm, F., Akkari, L., Pyonteck, S.M., Sevenich, L., Quail, D.F., Dhara, S., Simpson, K., Gardner, E.E., Iacobuzio-Donahue, C.A., et al. (2016). Macrophage ontogeny underlies differences in tumor-specific education in brain malignancies. Cell Rep. *17*, 2445–2459.

Brennan, C.W., Verhaak, R.G., McKenna, A., Campos, B., Noushmehr, H., Salama, S.R., Zheng, S., Chakravarty, D., Sanborn, J.Z., Berman, S.H., et al. (2013). The somatic genomic landscape of glioblastoma. Cell *155*, 462–477.

Burton, J.L., Madsen, S.A., Yao, J., Sipkovsky, S.S., and Coussens, P.M. (2001). An immunogenomics approach to understanding periparturient immunosuppression and mastitis susceptibility in dairy cows. Acta Vet. Scand. *42*, 407–424.

Buttgereit, A., Lelios, I., Yu, X., Vrohlings, M., Krakoski, N.R., Gautier, E.L., Nishinakamura, R., Becher, B., and Greter, M. (2016). Sall1 is a transcriptional regulator defining microglia identity and function. Nat. Immunol. *17*, 1397–1406.

Cancer Genome Atlas Research Network, Brat, D.J., Verhaak, R.G., Aldape, K.D., Yung, W.K., Salama, S.R., Cooper, L.A., Rheinbay, E., Miller, C.R., Vitucci, M., et al. (2015). Comprehensive, integrative genomic analysis of diffuse lower-grade gliomas. N. Engl. J. Med. *372*, 2481–2498.

Chen, Z., Feng, X., Herting, C.J., Garcia, V.A., Nie, K., Pong, W.W., Rasmussen, R., Dwivedi, B., Seby,

S., Wolf, S.A., et al. (2017). Cellular and molecular identity of tumor-associated macrophages in glioblastoma. Cancer Res. *77*, 2266–2278.

Cheng, L., Huang, Z., Zhou, W., Wu, Q., Donnola, S., Liu, J.K., Fang, X., Sloan, A.E., Mao, Y., Lathia, J.D., et al. (2013). Glioblastoma stem cells generate vascular pericytes to support vessel function and tumor growth. Cell *153*, 139–152.

Criscuoli, M.L., Nguyen, M., and Eliceiri, B.P. (2005). Tumor metastasis but not tumor growth is dependent on Src-mediated vascular permeability. Blood *105*, 1508–1514.

Dreher, M.R., Liu, W., Michelich, C.R., Dewhirst, M.W., Yuan, F., and Chilkoti, A. (2006). Tumor vascular permeability, accumulation, and penetration of macromolecular drug carriers. J. Natl. Cancer Inst. *98*, 335–344.

Eckel-Passow, J.E., Lachance, D.H., Molinaro, A.M., Walsh, K.M., Decker, P.A., Sicotte, H., Pekmezci, M., Rice, T., Kosel, M.L., Smirnov, I.V., et al. (2015). Glioma groups based on 1p/19q, IDH, and TERT promoter mutations in tumors. N. Engl. J. Med. *372*, 2499–2508.

Goldmann, T., Wieghofer, P., Jordao, M.J., Prutek, F., Hagemeyer, N., Frenzel, K., Amann, L., Staszewski, O., Kierdorf, K., Krueger, M., et al. (2016). Origin, fate and dynamics of macrophages at central nervous system interfaces. Nat. Immunol. *17*, 797–805.

Gomez Perdiguero, E., Klapproth, K., Schulz, C., Busch, K., Azzoni, E., Crozet, L., Garner, H., Trouillet, C., de Bruijn, M.F., Geissmann, F., et al. (2015). Tissue-resident macrophages originate from yolk-sac-derived erythro-myeloid progenitors. Nature *518*, 547–551.

Hambardzumyan, D., and Bergers, G. (2015). Glioblastoma: defining tumor niches. Trends Cancer *1*, 252–265.

Hambardzumyan, D., Gutmann, D.H., and Kettenmann, H. (2016). The role of microglia and macrophages in glioma maintenance and progression. Nat. Neurosci. *19*, 20–27.

Holash, J., Maisonpierre, P.C., Compton, D., Boland, P., Alexander, C.R., Zagzag, D., Yancopoulos, G.D., and Wiegand, S.J. (1999). Vessel cooption, regression, and growth in tumors mediated by angiopoietins and VEGF. Science *284*, 1994–1998.

Holland, E.C. (2000). A mouse model for glioma: biology, pathology, and therapeutic opportunities. Toxicol. Pathol. *28*, 171–177.

Holland, E.C., and Varmus, H.E. (1998). Basic fibroblast growth factor induces cell migration and proliferation after glia-specific gene transfer in mice. Proc. Natl. Acad. Sci. U S A *95*, 1218–1223.

Hoshide, R., and Jandial, R. (2016). 2016 world health organization classification of central nervous system tumors: an era of molecular biology. World Neurosurg. *94*, 561–562.

Ishisaki, A., Murayama, T., Ballagi, A.E., and Funa, K. (1997). Nuclear factor Y controls the basal transcription activity of the mouse platelet-derived-growth-factor beta-receptor gene. Eur. J. Biochem. *246*, 142–146.

Jain, R.K. (2014). Antiangiogenesis strategies revisited: from starving tumors to alleviating hypoxia. Cancer Cell *26*, 605–622.

Jiang, Y., Boije, M., Westermark, B., and Uhrbom, L. (2011). PDGF-B Can sustain self-renewal and tumorigenicity of experimental glioma-derived cancer-initiating cells by preventing oligodendrocyte differentiation. Neoplasia *13*, 492–503.

Jiang, Y., Marinescu, V.D., Xie, Y., Jarvius, M., Maturi, N.P., Haglund, C., Olofsson, S., Lindberg, N., Olofsson, T., Leijonmarck, C., et al. (2017). Glioblastoma cell malignancy and drug sensitivity are affected by the cell of origin. Cell Rep. *18*, 977–990.

Karrlander, M., Lindberg, N., Olofsson, T., Kastemar, M., Olsson, A.K., and Uhrbom, L. (2009). Histidine-rich glycoprotein can prevent development of mouse experimental glioblastoma. PLoS One *4*, e8536.

Kazlauskas, A. (2017). PDGFs and their receptors. Gene *614*, 1–7.

Kim, Y., Kim, E., Wu, Q., Guryanova, O., Hitomi, M., Lathia, J.D., Serwanski, D., Sloan, A.E., Weil, R.J., Lee, J., et al. (2012). Platelet-derived growth factor receptors differentially inform intertumoral and intratumoral heterogeneity. Genes Dev. *26*, 1247–1262.

Lindberg, N., Kastemar, M., Olofsson, T., Smits, A., and Uhrbom, L. (2009). Oligodendrocyte progenitor cells can act as cell of origin for experimental glioma. Oncogene *28*, 2266–2275.

Louis, D.N., Perry, A., Reifenberger, G., von Deimling, A., Figarella-Branger, D., Cavenee, W.K., Ohgaki, H., Wiestler, O.D., Kleihues, P., and Ellison, D.W. (2016). The 2016 world health organization classification of tumors of the central nervous system: a summary. Acta Neuropathol. *131*, 803–820.

Lu, F., Chen, Y., Zhao, C., Wang, H., He, D., Xu, L., Wang, J., He, X., Deng, Y., Lu, E.E., et al. (2016). Olig2-dependent reciprocal shift in PDGF and EGF receptor signaling regulates tumor phenotype and mitotic growth in malignant glioma. Cancer Cell *29*, 669–683.

Mazzone, M., Dettori, D., Leite de Oliveira, R., Loges, S., Schmidt, T., Jonckx, B., Tian, Y.M., Lanahan, A.A., Pollard, P., Ruiz de Almodovar, C., et al. (2009). Heterozygous deficiency of PHD2 restores tumor oxygenation and inhibits metastasis via endothelial normalization. Cell *136*, 839–851.

Mitew, S., Hay, C.M., Peckham, H., Xiao, J., Koenning, M., and Emery, B. (2014). Mechanisms regulating the development of oligodendrocytes and central nervous system myelin. Neuroscience *276*, 29–47.

Moeton, M., Kanski, R., Stassen, O.M., Sluijs, J.A., Geerts, D., van Tijn, P., Wiche, G., van Strien, M.E., and Hol, E.M. (2014). Silencing GFAP isoforms in astrocytoma cells disturbs laminin-dependent motility and cell adhesion. FASEB J. *28*, 2942–2954.

Molander, C., Hackzell, A., Ohta, M., Izumi, H., and Funa, K. (2001). Sp1 is a key regulator of the PDGF beta-receptor transcription. Mol. Biol. Rep. *28*, 223–233.

Ozawa, T., Riester, M., Cheng, Y.K., Huse, J.T., Squatrito, M., Helmy, K., Charles, N., Michor, F., and Holland, E.C. (2014). Most human non-GCIMP glioblastoma subtypes evolve from a common proneural-like precursor glioma. Cancer Cell *26*, 288–300.

Pyonteck, S.M., Akkari, L., Schuhmacher, A.J., Bowman, R.L., Sevenich, L., Quail, D.F., Olson, O.C., Quick, M.L., Huse, J.T., Teijeiro, V., et al. (2013). CSF-1R inhibition alters macrophage polarization and blocks glioma progression. Nat. Med. *19*, 1264–1272.

Quail, D.F., Bowman, R.L., Akkari, L., Quick, M.L., Schuhmacher, A.J., Huse, J.T., Holland, E.C., Sutton, J.C., and Joyce, J.A. (2016). The tumor microenvironment underlies acquired resistance to CSF-1R inhibition in gliomas. Science *352*, aad3018.

Quail, D.F., and Joyce, J.A. (2017). The microenvironmental landscape of brain tumors. Cancer Cell *31*, 326–341.

Reifenberger, G., Wirsching, H.G., Knobbe-Thomsen, C.B., and Weller, M. (2016). Advances in the molecular genetics of gliomas - implications for classification and therapy. Nat. Rev. Clin. Oncol. *14*, 434–452.

Rolny, C., Mazzone, M., Tugues, S., Laoui, D., Johansson, I., Coulon, C., Squadrito, M.L., Segura, I., Li, X., Knevels, E., et al. (2011). HRG inhibits tumor growth and metastasis by inducing macrophage polarization and vessel normalization through downregulation of PlGF. Cancer Cell *19*, 31–44.

Skalli, O., Wilhelmsson, U., Orndahl, C., Fekete, B., Malmgren, K., Rydenhag, B., and Pekny, M. (2013). Astrocytoma grade IV (glioblastoma multiforme) displays 3 subtypes with unique expression profiles of intermediate filament proteins. Hum. Pathol. *44*, 2081–2088.

Sorensen, M.D., Dahlrot, R.H., Boldt, H.B., Hansen, S., and Kristensen, B.W. (2017). Tumor-associated microglia/macrophages predict poor prognosis in high-grade gliomas and correlate with an aggressive tumor subtype. Neuropathol. Appl. Neurobiol. *44*, 185–206.

Tchougounova, E., Kastemar, M., Brasater, D., Holland, E.C., Westermark, B., and Uhrbom, L. (2007). Loss of Arf causes tumor progression of PDGFB-induced oligodendroglioma. Oncogene *26*, 6289–6296.

Uhrbom, L., Dai, C., Celestino, J.C., Rosenblum, M.K., Fuller, G.N., and Holland, E.C. (2002). Ink4a-Arf loss cooperates with KRas activation in astrocytes and neural progenitors to generate glioblastomas of various morphologies depending on activated Akt. Cancer Res. *62*, 5551–5558.

van den Bent, M.J., Brandes, A.A., Taphoorn, M.J., Kros, J.M., Kouwenhoven, M.C., Delattre,

J.Y., Bernsen, H.J., Frenay, M., Tijssen, C.C., Grisold, W., et al. (2013). Adjuvant procarbazine, lomustine, and vincristine chemotherapy in newly diagnosed anaplastic oligodendroglioma: long-term follow-up of EORTC brain tumor group study 26951. J. Clin. Oncol. *31*, 344–350.

Verhaak, R.G., and Valk, P.J. (2010). Genes predictive of outcome and novel molecular classification schemes in adult acute myeloid leukemia. Cancer Treat. Res. *145*, 67–83.

Wallerius, M., Wallmann, T., Bartish, M., Ostling, J., Mezheyeuski, A., Tobin, N.P., Nygren, E., Pangigadde, P., Pellegrini, P., Squadrito, M.L., et al. (2016). Guidance molecule SEMA3A restricts tumor growth by differentially regulating the proliferation of tumor-associated macrophages. Cancer Res. *76*, 3166–3178.

Zhang, X.M., Lund, H., Mia, S., Parsa, R., and Harris, R.A. (2014). Adoptive transfer of cytokine-induced immunomodulatory adult microglia attenuates experimental autoimmune encephalomyelitis in DBA/1 mice. Glia *62*, 804–817.

ISCI, Volume *9*

## Supplemental Information

# Microglia Induce PDGFRB Expression in Glioma Cells to Enhance Their Migratory Capacity

**Tatjana Wallmann, Xing-Mei Zhang, Majken Wallerius, Sara Bolin, Anne-Laure Joly, Caroline Sobocki, Lina Leiss, Yiwen Jiang, Jonas Bergh, Eric C. Holland, Per Ø. Enger, John Andersson, Fredrik J. Swartling, Hrvoje Miletic, Lene Uhrbom, Robert A. Harris, and Charlotte Rolny**

**Figure S1**

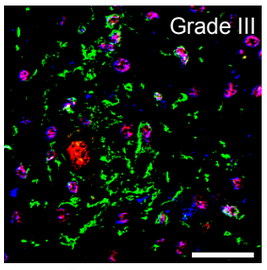


IDH1-R132H α-SMA IBA1

SUPPLEMENTAL FIGURE LEGEND

**Figure S1. [α-SMA$^+$ glioma cells are in close proximity to IBA1$^+$ TAMMs], Related to Figure 4.**

Human Grade III astrocytoma sections were immunostained for IDH1-R132H (blue), α-SMA (red) and IBA1 (green). Bars 50 μm.

**Figure S2**

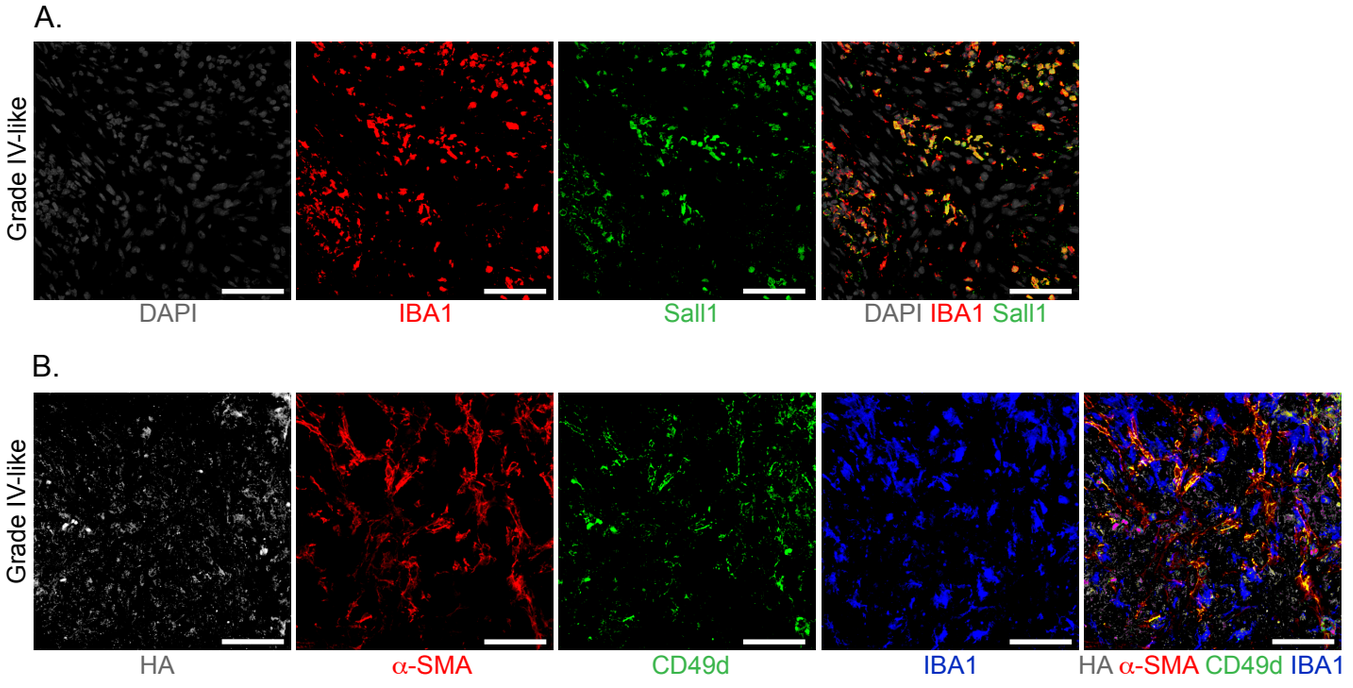
A.
Grade IV-like
DAPI
IBA1
Sall1
DAPI IBA1 Sall1
B.
Grade IV-like
HA
α-SMA
CD49d
IBA1
HA α-SMA CD49d IBA1

SUPPLEMENTAL FIGURE LEGEND

**Figure S2. [IBA1$^{+}$ TAMMs express Sall1], Related to Figure 5.**

(A) Mouse Grade IV-like glioma sections were immunostained for DAPI (grey), IBA1 (red) and Sall1 (green). Bars 50 μm.

(B) Mouse Grade IV-like glioma sections were immunostained for HA (grey), α-SMA (red), CD49d (green) and IBA1 (blue). Bars 50 μm.

**TABLE S1. [Quantitative PCR Probes], Related to Figure 6.**

TaqMan probes (Life Technologies)

| | |
|---|---|
| *α-sma* | Mm00725412_s1 |
| *pdgfrb* | Mm00435546_m1 |
| *β-actin* | Mm00607939_s1 |
| *cxcl9* | Mm00434946_m1 |
| *cxcl10* | Mm00445235_m1 |
| *cxcl11* | Mm00444662_m1 |
| *il-6* | Mm00446190_m1 |
| *il-1b* | Mm01336189_m1 |
| *arginase1* | Mm00475988_m1 |
| *mrc1* | Mm01329362_m1 |
| *ym1* | Mm00657889_mH |

SYBR green probes (Sigma)

| | |
|---|---|
| *pdgfra* | FW 5'-ATATTTGAGACATTGCTGGC<br>RW 5'-CTAGTTCCTGCATCCATTTTG |
| *egfr* | FW 5'-CTGTCGCAAAGTTTGTAATG<br>RW 5'-GAATTTCTAGTTCTCGTGGG |
| *fgfr* | FW 5'-TATGTCCAGATCCTGAAGAC<br>RW 5'-GAGAGTCCGATAGAGTTACC |
| *hgfr* | FW 5'-CGACAAATACGTTGAAATGC<br>RW 5'-GATCTACATAGGAGAATGCAC |
| *igf-1r* | FW 5'-AGAACCGAATCATCATAACG<br>RW 5'-TTTTAAATGGTGCCTCCTTG |
| *cnp* | FW 5'-CTTCGACACTTTATTTCTGGAG<br>RW 5'-AATTTGGTTGTACAGTGCAG |
| *gfap* | FW 5'-GGAAGATCTATGAGGAGGAAG<br>RW 5'-CTGCAAACTTAGACCGATAC |

| | |
|---|---|
| *hes1* | FW 5'-AAGCCTATCATGGAGAAGAG<br>RW 5'-GGAGCTATCTTTCTTAAGTGC |
| *ng2* | FW 5'-GGCAGCACTGCCTCCTGGAC<br>RW 5'-CCCTGGCCCCACTGCAACTG |
| *β-actin* | FW 5'-GATGTATGAAGGCTTTGGTC<br>RW 5'-TGTGCACTTTTATTGGTCTC |

SYBR green probes (QIAGEN)

| | |
|---|---|
| *nestin* | QT00316799 |
| *olig2* | QT01041089 |
| *sox2* | QT02249347 |

TRANSPARENT METHODS

**Mouse tumor models**

We used a PDGF-B-driven replication-competent leukosis virus splice acceptor (RCAS)/*tv-a* mouse glioma model in which transgenic expression of the avian tv-a receptor expression is under the nestin (NES) promoter (Holland and Varmus, 1998) in a homozygous p19Arf-deficient ($Arf^{-/-}$) background and denoted *N/tv-a;*$Arf^{-/-}$ mice (Tchougounova et al., 2007). In order to induce glioma, $4\times10^5$ RCAS virus-encoding PDGF-B-producing DF-1 chicken fibroblasts were transplanted through intracerebral injections into neonatal mice. RCAS is replication incompetent in mammalian cells and infection of nestin-expressing target cells will occur during the first days after injection. Within three months injected mice will develop gliomas with different degree of malignancies (Karrlander et al., 2009; Tchougounova et al., 2007). Experiments were conducted in accordance with the local Animal Ethics Committee decision C300/10.

**Patient glioma material**

Paraffin-embedded human astrocytoma samples were obtained from the Research Biobank for intracranial neoplasms at Bergen University, Bergen, Norway. Surgical specimens were collected during surgical resections at the Department of Neurosurgery, Haukeland Univeristy Hospital, Bergen, Norway. All material in the Research Biobank was collected with written informed consent from patients and the Biobank is approved by the regional ethical committee (013.09, 2013/720 and 2018/1520).

**Histological analysis**

Tumor samples embedded in paraffin or in OCT were cut in 6µm or 10µm thick sections, and stained as previously described (Wallerius et al., 2016). Tumor

sections were stained with hematoxylen harris and eosin (HistoLab) or treated for antigen retrival with sodium citrate buffer (Thermo Scientific Fisher and Biocare Medical) and immunostained with appropriate antibodies: anti-CD31 (Santa Cruz), Podocalyxin (R&D systems), α-SMA (Sigma), PDGFRB (Cell Signalling and Abcam), CD44 (Santa Cruz), Sox2, GFAP, Olig2 and NG2 (Millipore), Ki67 (Abcam), MRC1 (CD206; AbD), Iba 1 (Wako chemicals and Abcam), HA (Acris and Abcam), GFAP (Abcam), IDH-R132H (Dianova); streptavidin and all secondary antibodies were conjugated with AlexaFluor 405, AlexaFluor 488, AlexaFluor 546, AlexaFluor 555 or AlexaFluor 647 fluorochromes (Molecular Probes). Cell nuclei were labeled with DAPI (Invitrogen Corp). Tumor hypoxia was detected by intraperitoneal injection of 60mg/kg pimonidazole hydrochloride (HypoxiProbe) into tumor-bearing mice. Vessel functionality was assessed by intravenous injection of 1mg of FITC-conjugated lectin (Molecular Probes) into tumor-bearing mice (this compound binds to the inner lumen of vessels) (Criscuoli et al., 2005; Dreher et al., 2006). Ten minutes later mice were sacrificed and their brains were fixed in 4% formalin and embedded in paraffin or in OCT embedding material and frozen in isobutanol on dry ice. At least 6 independent fields from sections from each tumor were analyzed by using LSM 510 META, LSM700 META and LSM T-PMT Zeiss confocal microscopes and quantified using ImageJ software.

**Primary mouse glioma cells**

The cultured mouse glioma stem cells were derived from RCAS-PDGF-B-induced grade IV gliomas in *N/tv-a;Arf*$^{-/-}$ mice (Jiang et al., 2017) and cultured under stem cell conditions as previously described (Jiang et al., 2011). These cells have all functional characteristics of GBM stem cells and will be denoted GSCs.

**Isolation of microglia**

6-to-8-week-old naïve mice were deeply anesthetized and perfused with ice-cold PBS (Sigma). Brains were removed without meninges, enzymatically digested and resuspended in 0.5 mg/ml DNaseI in HBSS. Cell pellets were resuspended in DMEM/F12 complete (complemented with 10% FBS, 1% Penicillin Streptomycin (P/S, 100 units/ml) and 1% Glutamine (100µg/ml, Sigma) supplemented with Macrophage Colony Stimulating Factor (M-CSF) (20ng/ml, Miltenyi) and cultured at 37°C and 5% $CO_2$. The primary cells were cultured until 80% confluence. Microglia were isolated with CD11b magnetic microbeads (Miltenyi Biotec 130-049-601) according to the manufacturer's instructions and seeded in DMEM/F12 medium complete supplemented with 50ng/ml M-CSF (Zhang et al., 2014).

**Isolation of BMDMs**

Bone marrow precursors were acquired by flushing the bone marrow from the femurs and tibias of 6-to-8-week-old naïve BALB/c mice. Erythrocytes were lysed with red blood cell lysis buffer (RCB, Sigma) and cells were cultured in RPMI-1640 medium supplemented with 10% FBS, 1% P/S (Gibco), 1% Glutamine (Gibco) and 50ng/ml M-CSF (Miltenyi) for 6-to-7 days (Wallerius et al., 2016).

**M1- or M2- polarized microglia and BMDMs**

Microglia or BMDMs were polarized to either an M1-phenotype (100 ng/ml LPS (Sigma) and 200 units/ml IFNγ (Peprotech)) or an M2-phenotype (20 ng/ml IL-4 (Peprotech), 10 ng/ml TGF-β (Peprotech), 20 ng/ml IL-10 (R&D)) for 24 hours.

**Co-culture experiments**

M1- and M2-polarized microglia or M1- and M2-polarized BMDMs were washed two times with PBS before N/tv-a PDGF-B $GFP^+$GCSs were added and co-cultured with or without M1- or M2-polarized microglia or M1- or M2-polarized BMDMs for 24h at

37°C. Control medium (M0) or conditioned medium from M1- or M2-polarized microglia was added to N/tv-a PDGF-B GFP$^+$GCSs for 24 h at 37°C. GFP$^+$GCSs were then flow-sorted and subjected to RNA isolation and cDNA synthesis.

**RNA Extraction, cDNA Synthesis and quantitative RT-PCR**

Total RNA was extracted from N/tv-a PDGF-B GFP$^+$GCSs, microglia or BMDMs. Cells were collected in RLT buffer and RNA was extracted and cDNA synthesized from collected glioma cells, microglia or BMDMs as previously described. Gene expression was analyzed by performing quantitative RT-PCR. TaqMan and SyBr green probes are listed in Supplemental table 1.

**Migration Assay**

The mouse glioma cells were co-cultured with M1- or M2-polarized microglia for 8h before they were seeded on laminin (5 μg/ml)-coated transwell membranes (VWR) +/- 10 μg/ml PDGFRB neutralizing antibody (ThermoFisher) for 24h at 37°C. Cells in the upper part of the membrane were removed. The membranes were fixed in 4% paraformaldehyde and immunostained with an Olig2 antibody (Millipore) and the appropriate secondary antibody conjugated with AlexaFluor 488 (Molecular Probes). Cell nuclei were labeled with DAPI. Cells were counted using a LSM T-PMT Zeiss confocal microscope and quantified using ImageJ software.

**Statistical analysis**

In all studies, values are expressed as Standard Deviation (SD) and mean. Statistical analyses were performed using One-way ANOVA. Stars and hash tags in the graphs indicate significance as depicted in figure legends. Differences were considered statistically significant at $p<0.05$.